Explanation of anomalous polariton dynamics in $LiTaO_3$

Gary P. Wiederrecht,* Thomas P. Dougherty,† Lisa Dhar, and Keith A. Nelson
Department of Chemistry, Massachusetts Institute of Technology, Cambridge, Massachusetts 02139

D. E. Leaird and A. M. Weiner‡
Bell Communications Research, 331 Newman Springs Road, Red Bank, New Jersey 07701-7040
(Received 2 May 1994)

Single and multiple-pulse impulsive stimulated Raman-scattering (ISRS) experiments are used to investigate the anomalously high damping rates of the lowest frequency A_1 polariton in $LiTaO_3$. The wave-vector dependence of the response reveals coupling of the polariton to a weakly Raman-active, low-frequency relaxational mode as well as to two underdamped modes of a different symmetry. Inclusion of the coupled modes yields quantitative agreement between the results and the predictions of a previously developed theory for light scattering from polaritons.

I. INTRODUCTION

The ferroelectric material lithium tantalate ($LiTaO_3$) is of interest for a variety of nonlinear optical applications, such as electro-optic modulation and harmonic generation. It is easily grown with high optical quality and has a relatively large electro-optic coefficient (2.5×10^{-11} m/V) along its optical axis.[1] The electro-optic and ferroelectric properties of $LiTaO_3$ (Ref. 2) as well as other crystals[3] are known to be heavily mediated by low-frequency lattice vibrations (with energies less than 200 cm^{-1}). However, $LiTaO_3$ is a more complicated system from a phonon dynamical point of view than other well studied perovskite crystals such $BaTiO_3$ and $KNbO_3$. There are two formula units per unit cell, increasing the number of optic phonons from 12 to 27. The lone paraelectric-ferroelectric phase transition occurs at a relatively high-temperature T_c of 620 °C.

$LiTaO_3$ has C_{3v} symmetry with two formula units per unit cell and should have four phonons with A_1 symmetry and nine phonons with E symmetry. The low-frequency phonons in $LiTaO_3$ below 200 cm^{-1} have been particularly difficult to characterize accurately, despite many studies of the material with a variety of experimental techniques.[2,4–14] The lowest frequency A_1 mode at low wave vectors is a dispersive phonon-polariton mode.[7,11–14] There has been considerable disagreement in the assignments and reported frequencies of the low-frequency modes which are light-scattering active. Kaminow and Johnston[2,4] reported a Raman-scattering study of $LiTaO_3$ and assigned the lowest frequency A_1 transverse optic mode to 201 cm^{-1} and the lowest frequency E-symmetry modes at 74 and 140 cm^{-1}. They also demonstrated the presence of strain in their crystals by measuring birefringence along the nominally equivalent axes, and showed a correlation between the magnitude of the strain and the strength of the disallowed E modes in the A_1 symmetry spectra.[2,4] An area of continuing disagreement through the years has been the assignment of these low-frequency E modes. Barker, Ballman, and Ditzenberger[5] performed infrared reflectivity measurements and found no evidence for a mode near 80 cm^{-1}. They instead tentatively reported a weak mode at 165 cm^{-1}. More recent light-scattering experiments have also shown little evidence for the mode at 80 cm^{-1}, or have attributed a peak in this region to two-phonon effects.[9,10] One group found strong evidence for a mode at 81 cm^{-1}, but assigned the mode to A_1 symmetry and concluded that the spectra indicated C_3 symmetry for the crystal.[7] Still another group[8] reported a "quasimode" at 106 cm^{-1}. In addition to these discrepancies, large differences in the linewidths of the modes have been observed. The results of previous experiments are summarized in Table I.

Two femtosecond time-resolved studies of $LiTaO_3$ have been reported recently. Auston and Nuss observed anomalies in the absorption spectrum of the polariton generated through the inverse electro-optic effect.[11,12] They suggested that a peak in the absorption of the polariton resulted from coupling to a weak two-phonon process. Coupling to other normal modes of different symmetry was also suggested. This is a viable proposition due to the evidence discussed above that strain can break the zero-order symmetry of the crystal and lend some degree of A_1 character to E-symmetry modes.[2,6] Very recently, Bakker, Hunsche, and Kurz observed a polariton beating pattern near a wave vector of 1010 cm^{-1} and an avoided crossing at a polariton frequency of 31 cm^{-1}. They attributed this avoided crossing to a resonance due to tunneling of the Li ion between two potential energy wells in the unit cell.[14]

In an effort to add further insight into the anomalous behavior of the low-frequency spectrum in $LiTaO_3$, we have performed time-resolved impulsive stimulated Raman-scattering (ISRS) experiments on the A_1 polariton as a function of excitation wave vector. Though the wave-vector dependence of the polariton frequency has been reported previously, this study includes an accurate measurement of the polariton linewidth dispersion. Because the damping rate is considerably more sensitive

0163-1829/95/51(2)/916(16)/$06.00

TABLE I. Previous measurements of the frequency and damping of the lowest frequency A_1 phonon and the E-symmetry modes below 200 cm^{-1} are shown. A wide spread in the results is evident.

Ref.	Frequency of E-symmetry modes	Linewidth of E-symmetry modes	Frequency of A_1 (TO) phonon	Linewidth of A_1 (TO) phonon
2	74 (TO)	19	201	15
	80 (LO)	12		
	140 (TO)	6		
	163 (LO)	6		
5	142 (TO)	14	200	28
	165 (LO,TO)	11		
	175 (LO,TO)	7		
7	69 (TO)	21	202	26
	70 (LO)			
	141 (TO)	10		
	200 (LO)			
9	142 (TO)		206	
	190 (LO)			
10	142 (TO)		203	
	190 (LO)			

than the frequency to mode-mode interactions, the measurement of the polariton linewidth dispersion can elucidate the coupling of other modes to the polariton mode. We observe two peaks in the wave-vector-dependent polariton damping rate, at polariton frequencies of 92 and 140 cm^{-1}, indicating bilinear coupling to other phonon modes of those frequencies. In addition, the greatest deviation of the polariton damping rate from that predicted from a single polar mode model occurs for polariton frequencies below 60 cm^{-1}, where the experimentally observed values differ by factors of 5 or more. This indicates coupling to a weakly Raman-active relaxational mode. No evidence for the avoided crossing at 31 cm^{-1} reported recently[14] is found. A mode-coupling model is developed that explains the wave-vector dependence of the polariton damping rates and also the unusual wave-vector dependence of the polariton ISRS signal intensity.

Most of the experiments reported were conducted at room temperature. ISRS experiments at reduced temperatures were difficult due to photorefractive effects which make $LiTaO_3$ sensitive to visible laser light. These effects are rapidly reversible at room temperature, but are very long-lived at low temperatures. In order to reduce the peak light intensity at low temperatures, ISRS experiments were conducted with a timed sequence of excitation pulses rather than with a single pair of excitation pulses to avoid photorefractive damage. The sequence of pulses was used to repetitively drive the phonon-polariton mode such that its coherent amplitude was sufficient for detection by the probe pulse. In this manner the polariton properties could be characterized without the use of a single, intense pair of excitation pulses which give rise to photorefractive damage. The results of the low-temperature multiple-pulse ISRS experiments are also explained in terms of the mode-coupling model.

II. ISRS TECHNIQUE APPLIED TO $LiTaO_3$

Experiments were conducted with a time-delayed four-wave mixing or "transient grating" geometry as shown in the inset to Fig. 1. The sudden ("impulse") driving force exerted by crossed ultrashort excitation pulses on Raman-active modes through impulsive stimulated Raman scattering (ISRS) has been discussed extensively.[15–18] If only one mode α with normal coordinate Q is involved, then the force exerted by the crossed pulses is given by

$$F^{(\alpha)}(t)=\frac{\partial\varepsilon}{\partial Q}F(t)\ , \tag{1}$$

where ε is the dielectric constant (treated as a scalar quantity because only one component, ε_{11}, is examined in these experiments), $d\varepsilon/dQ$ is the Raman-scattering differential polarizability, and $F(t)$ describes the excitation intensity profile. The response of the mode is given by

$$Q(t)=\int dt' G^{(\alpha)}(t-t')F^{(\alpha)}(t')\ , \tag{2}$$

where $G^{(\alpha)}(t)$ is the impulse response (Green's) function describing the dynamics of the mode. The sudden force exerted by the excitation pulses initiates time-dependent oscillations and decay of underdamped modes, which are monitored through coherent scattering of variably delayed probe pulses. The time-dependent response of overdamped and relaxational modes are discussed in Ref. 15. The time-dependent response given by Eq. (2) is observed through its effect on the dielectric constant:

$$\delta\varepsilon(t)=\sum_{\alpha}\frac{\partial\varepsilon}{\partial Q^{(\alpha)}}Q^{(\alpha)}(t)\ , \tag{3}$$

which can also be described in terms of the dielectric

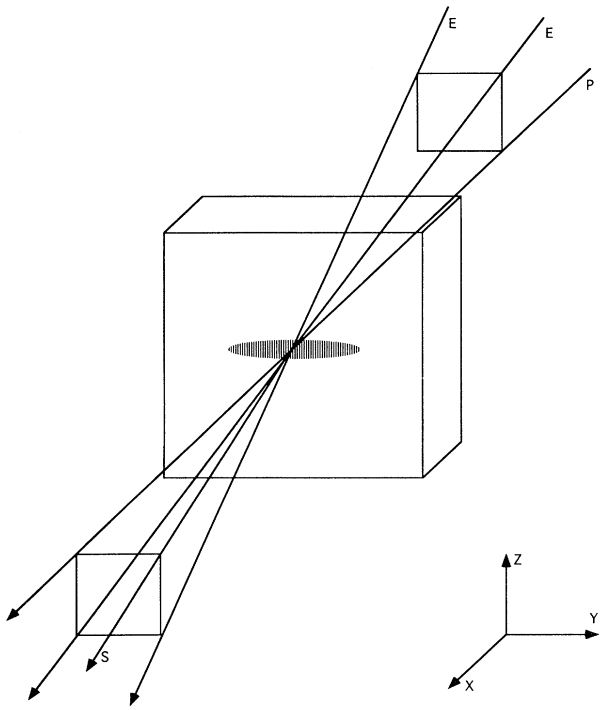

FIG. 1. An illustration of the ISRS geometry relative to the $LiTaO_3$ crystal axes. For excitation of the A_1 polariton, all beams are polarized along the polar (z) axis and the wave vector is parallel to y.

response function

$$G^{\varepsilon\varepsilon}(t)=\sum_{\alpha}\left[\frac{\partial\varepsilon}{\partial Q^{(\alpha)}}\right]^2 G^{(\alpha)}(t)\ , \tag{4}$$

through the relation

$$\delta\varepsilon(t)=\int dt' G^{\varepsilon\varepsilon}(t-t')F(t')\ . \tag{5}$$

Again the dielectric constant ε and its response function $G^{\varepsilon\varepsilon}(t)$ and differential polarizabilities $\delta\varepsilon/\delta Q^{(\alpha)}$ are written in scalar form for simplicity, since only one component of each (ε_{11} and $G^{\varepsilon\varepsilon}_{1111}$) is examined below. Assuming ideal time resolution, the time-dependent ISRS signal takes the form

$$I(t)\propto|G^{\varepsilon\varepsilon}(t)|^2\propto|\delta\varepsilon(t)|^2\ . \tag{6}$$

If several coupled modes are excited, then the driving force on each is given by Eq. (1) and the dielectric response is given by a sum of terms like that in Eq. (3). The response of each mode is given by

$$Q^{(\alpha)}(t)=\int dt'\sum_{\beta}G^{\alpha\beta}(t-t')F^{(\beta)}(t')\ , \tag{7}$$

where $G^{(\alpha\beta)}$ is a coupled-mode response function. The dielectric constant response function is related to the individual and coupled-mode response functions through the expression

$$G^{\varepsilon\varepsilon}(t)=\sum_{\alpha,\beta}\frac{\partial\varepsilon}{\partial Q^{(\alpha)}}\frac{\partial\varepsilon}{\partial Q^{\beta}}G^{(\alpha\beta)}(t)\ . \tag{8}$$

For $LiTaO_3$, we anticipate ISRS responses from two modes, one vibrational and one relaxational. In this case

$$G^{\varepsilon\varepsilon}(t)=Ke^{-\gamma t}\sin(\omega t+\phi)+Le^{-\lambda t}\ . \tag{9}$$

If the two modes are uncoupled, then $\phi=0$ and the two terms on the right-hand side of Eq. (9) are the uncoupled vibrational and relaxational response functions. If the modes are coupled then all the constants K, L, ϕ, γ, ω, and λ depend on the uncoupled dynamical parameters for both modes as well as the coupling strength. In either case, the time dependence of the data (assuming ideal time resolution) is given by the square of $G^{\varepsilon\varepsilon}(t)$ as is given in Eq. (6). The signal consists of damped oscillations and a nonoscillatory relaxational term. Note that if L is vanishingly small, then from Eq. (6) it follows that the signal intensity oscillates at twice the phonon frequency and decays at twice the phonon damping rate. On the other hand, if L exceeds K then the signal may show relaxation which is modulated by oscillations at the fundamental phonon frequency and damping rate due to the heterodyne (KL) term, i.e., the cross product of the oscillatory and relaxational terms.

The effects of finite excitation and probe-pulse durations on ISRS signal have been discussed previously.[15,16] The material responses are described by Eqs. (1), (2), (5), and (7) in which the forcing terms contain the excitation pulse temporal profile. The signal is a convolution of the dielectric response given in Eq. (5) with the temporal profile $P(t)$ of the probe pulse, i.e.,

$$I(t)=\int_{-\infty}^{\infty}|\delta\varepsilon(t')|^2P(t-t')dt'\ . \tag{10}$$

Assuming identical temporal profiles for excitation and probe pulses with the Gaussian form,

$$F(t)=\frac{1}{\tau_{\text{pulse}}\sqrt{\pi}}e^{-t^2/\tau^2_{\text{pulse}}}\ , \tag{11}$$

the result of the convolution for the two modes described above can be expressed analytically for times after the excitation pulses have passed through the sample (i.e., for $t\gg\tau_{\text{pulse}}$) as

$$\begin{aligned}\delta\varepsilon(t)&=K\exp\left[\frac{\tau^2_{\text{pulse}}(\gamma^2-\omega^2)}{4}\right]\exp(-\gamma t)\sin\left[\omega t-\frac{\omega\gamma\tau^2_{\text{pulse}}}{2}\right]+L\exp\left[\frac{\lambda^2\tau^2_{\text{pulse}}}{4}\right]\exp(-\lambda t)\\&\approx K\exp\left[\frac{-\tau^2_{\text{pulse}}\omega^2}{4}\right]\exp(-\gamma t)\sin\left[\omega t-\frac{\omega\gamma\tau^2_{\text{pulse}}}{2}\right]+L\exp(-\lambda t)\end{aligned} \tag{12}$$

and

$$
\begin{aligned}
I(t)=&\frac{K^2}{2}\exp\left[-2\gamma t+\frac{3\gamma^2\tau_{\text{pulse}}^2}{2}-\frac{\tau_{\text{pulse}}^2\omega^2}{2}\right][1-\exp(-\omega^2\tau_{\text{pulse}}^2)\cos(2\omega t-3\omega\gamma\tau_{\text{pulse}}^2)]\\
&+KL\exp\left[-(\gamma+\lambda)t+\frac{\lambda\gamma\tau_{\text{pulse}}^2}{2}+\frac{\lambda^2\tau_{\text{pulse}}^2}{2}+\frac{(\gamma^2+\omega^2)\tau_{\text{pulse}}^2}{2}\right]\\
&\times\sin\left[\omega t-\omega\gamma\tau_{\text{pulse}}^2-\frac{3\lambda^2\tau_{\text{pulse}}^2}{2}\right]+L^2\exp\left[-2\lambda t+\frac{3\lambda^2\tau_{\text{pulse}}^2}{2}\right]\\
\approx&\frac{K^2}{2}\exp(-2\gamma t)\exp\left[-\frac{\tau_{\text{pulse}}^2\omega^2}{2}\right][1-\exp(-\omega^2\tau_{\text{pulse}}^2)\cos(2\omega t-3\omega\gamma\tau_{\text{pulse}}^2)]\\
&+KL\exp[-(\gamma+\lambda)t]\exp\left[\frac{-\omega^2\tau_{\text{pulse}}^2}{2}\right]\sin\left[\omega t-\omega\gamma\tau_{\text{pulse}}^2-\frac{3\lambda^2\tau_{\text{pulse}}^2}{2}\right]+L^2\exp(-2\lambda t)\ ,
\end{aligned}
\tag{13}
$$

where the approximate expressions are valid for small damping rates, i.e., $\gamma \ll \omega$, small relaxational decay rates, i.e., $\lambda \ll \omega$, and pulse durations which are short at least compared to the decay times, i.e., $\tau_{\text{pulse}} < \gamma^{-1}, \lambda^{-1}$. The phase factor ϕ of Eq. (9) is no longer included as it was not experimentally observed in the present experiments. The approximate expression (12) shows that the vibrational mode can be excited "impulsively" until the pulse duration approaches the vibrational oscillation period, i.e., the value $\omega^2\tau_{\text{pulse}}^2/4=1$ is approached. However in the approximate expression (13) for the intensity of the signal we see that the oscillatory part of the first (K^2) term becomes weak in intensity at somewhat shorter pulse durations, where oscillations at twice the phonon frequency can no longer be time resolved even if they can be impulsively excited. Even when these oscillations in the signal are lost, the K^2 term still yields a signal which decays at twice the vibrational damping rate. If the magnitude of L is extremely small, then the data show decaying oscillations for sufficiently short pulses, only a monotonic decay if the pulse duration is slightly too long, and finally no signal at all for long pulse durations. If the magnitude of L is sufficient, then because of the (KL) heterodyne term in Eq. (13), oscillations at the fundamental frequency may appear even when the oscillations at twice the frequency can no longer be time resolved. For still longer pulse durations, such that $\omega^2\tau_{\text{pulse}}^2 > 1$, only the relaxational mode decay can be observed.

A phonon-polariton mode is inherently dispersive in character, increasing in frequency as a function of wave vector. This suggests that the same trends described above for different pulse durations should be observed as a function of wave vector. If L is negligibly small, then at small wave vector (corresponding to low phonon-polariton frequency), we may expect to see oscillations in ISRS signal at frequency 2ω which decay at rate 2γ, while at somewhat larger wave vectors (reached experimentally by increasing the angle between excitation pulses), only a monotonic decay at rate 2γ is observed. At still larger wave vectors there may be no signal at all. If the relaxational mode is weakly coupled to the polariton mode or weakly Raman active (i.e., $L < K$), then at small wave vectors oscillations at frequency 2ω may be observed, at somewhat higher wave vectors oscillations should appear at the fundamental frequency ω, and at still higher wave vectors the oscillations should disappear entirely. The relevance of this case to our experiments will be discussed below. It will be shown that not only the polariton frequency but also its damping rate γ, the relaxational mode decay rate λ, and the amplitude values K and L may all be strongly dispersive. Thus wave-vector dependence of the ISRS data is due to both the pulse duration and the dispersive behavior of polaritons.

III. EXPERIMENTAL

Impulsive stimulated Raman scattering from polaritons has recently been demonstrated and discussed in detail.[3,13,19] The experimental geometry used here is shown in Fig. 1. The $LiTaO_3$ crystal, obtained from Inrad, is a 1-mm-thick x-cut sample, and is 5 mm square. To observe the transverse optic A_1 polariton, the wave vector is aligned along the y axis with the polarizations of all beams along the polar axis, designated as z. The excitation wave-vector magnitude is determined by the angle θ between the excitation beams (of wavelength λ_{laser}) in air through the relation

$$q=\frac{4\pi\sin(\theta/2)}{\lambda_{\text{laser}}}\ . \tag{14}$$

The angles were measured by reflecting one excitation beam upon the other through the use of a mirror mounted upon a rotational stage with one minute accuracy.

An important adaptation of the experimental setup for dispersive modes, also used for examination of acoustic phonons,[15] is cylindrical focusing of the excitation beams to form an excitation pattern which is wide (about 1.2 mm, compared to 120 μm high) in the grating wave-vector direction. This is done to prevent propagation of the polariton out of the excitation region before it is fully damped. For example, in the limit of small q, the group velocity, $v_g = d\omega/dq$, is $c/(\varepsilon_0)^{1/2}$, which is approximately 40 μm/psec for a typical low-frequency dielectric constant ε_0 of 50. A spot size exceeding 1 mm in the grating wave-vector direction permits accurate measurement of polariton decay times up to 25 ps, which is sufficient for the A_1 polariton in $LiTaO_3$. If the spot size is too small,

propagation effects result in a nonexponential decay of the signal.[13] Another way to look at this is as follows: a small beam has a range of q vectors which leads to artificially fast dephasing due to the dispersive nature of the polariton mode.

The experimental apparatus has been described in detail elsewhere.[20] Briefly, the system consists of a cw mode-locked Nd:YAG laser that synchronously pumps an antiresonant ring dye laser. The output of the dye laser consists of 80-fs pulses centered at 615 nm. The pulses are subsequently amplified by a three-stage dye amplifier which is synchronously pumped by the frequency-doubled output of a Q-switched, mode-locked, cavity-dumped Nd:YLF laser. The final output consists of 5-μJ pulses at a 500-Hz repetition rate. The pulse duration remains at 80 fs, but dispersion in the sample results in actual time resolution of approximately 120 fs.

IV. RESULTS

Data from the A_1 polariton mode in $LiTaO_3$ are shown in Fig. 2. The data at this wave vector ($q=1800$ cm^{-1}) can be fit with a single oscillator response function, i.e., the signal oscillates at twice the polariton frequency and decays at twice the polariton decay rate. A detailed description of the simulation of the data is described in Sec. V B 2. The frequency and damping rate of the polariton are 47.5 and 2.0 cm^{-1}, respectively. Data recorded throughout the wave-vector range between 900 and 6000 cm^{-1} are all well described by single damped oscillator response functions. The frequency increases monotonically with q as expected for a phonon-polariton mode and is discussed further below. Convolutions over the pump and probe-pulse durations were used to simulate all the data. Final fits were obtained with a Marquardt-Levenberg least-squares fitting routine.

Despite careful searching, no evidence was found for an avoided crossing which according to a recent report[14] occurs at $q=1300$ cm^{-1}. In particular, the ISRS data exhibited only single-frequency oscillations (i.e., no beating patterns indicative of two low-frequency modes) at all wave vectors.

In the wave-vector range of $q=6000$ cm^{-1} and $q=9000$ cm^{-1}, polariton oscillations at twice the polariton frequency can no longer be time resolved even though the mode can still be driven by the excitation pulses. Typical data are shown in Fig. 3. The signal is well described as a single exponential decay, which allows for an accurate measure of the polariton damping rate in this region. Fits were still carried out using a damped-oscillator response function with convolution over the pulse durations. As discussed below, theoretically predicted frequency values were used for the fits, and the damping rates obtained were relatively insensitive to these values.

At wave vectors above $q=9000$ cm^{-1}, oscillatory character returns to the data as shown in Fig. 4 for $q=12\,800$ cm^{-1}. The simulation of the data is described in Sec. V B 2. The oscillations, which are more strongly damped than at lower wave vectors, are at the fundamental polariton frequency rather than at twice the frequency. This indicates that a heterodyne term has been introduced at higher wave vectors. It is highly suggestive of a relaxational mode of A_1 symmetry whose contribution to the observed signal [represented by the $L\exp(-\lambda t)$ in Eq. (12)] grows at higher wave vectors. Polariton frequencies were obtained in this q region through fits based on the coupled-mode response given in Eq. (9), including convolution over the pulse durations as indicated in Eq. (13). No significant phase shifts were measured at any wave vector, so the phase factor ϕ was set to zero in the fitting procedure.

The wave-vector-dependent polariton frequencies and dephasing rate are shown in Fig. 5. As mentioned above,

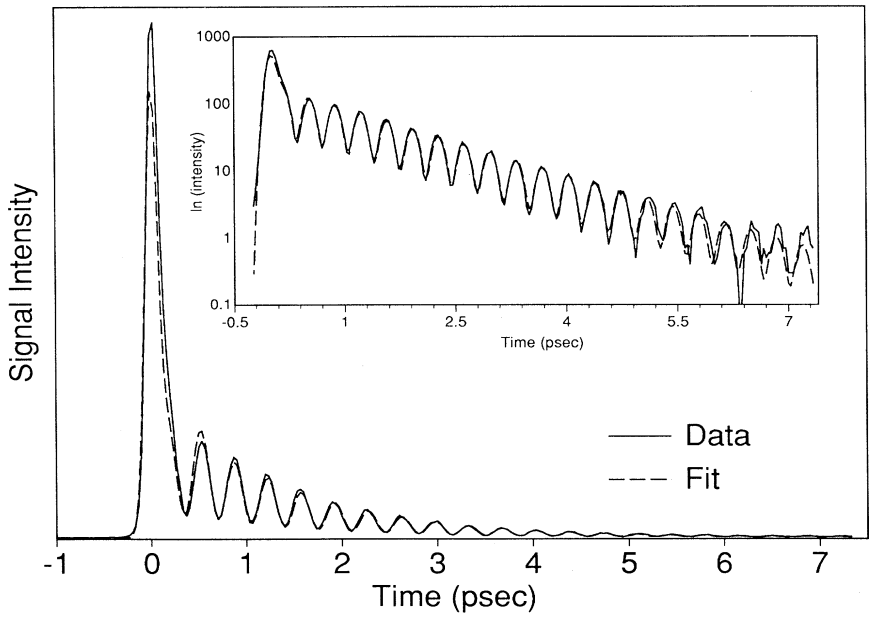

FIG. 2. ISRS signal from the A_1 polariton at $q=1800$ cm^{-1} along with a fit to the data with a single damped oscillator. The fit includes the nonresonant electronic response at $t=0$.

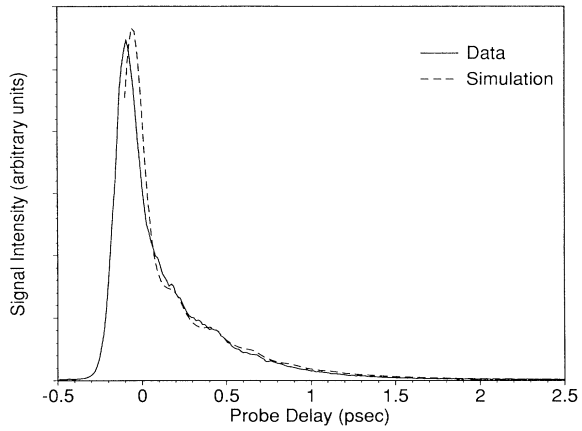

FIG. 3. ISRS signal from the A_1 polariton at $q=7000\ \mathrm{cm}^{-1}$. Convolution effects with the probe pulse wash out the oscillations, resulting in a smooth exponential decay of the signal.

the frequency increases monotonically with q. The dephasing rate (assumed hereafter to be the damping rate) generally increases with increasing q, but shows two sharp peaks at intermediate wave vectors. It also shows a somewhat unusual form at low wave vectors. These features will be discussed below.

V. DISCUSSION

Though the wave-vector-dependent coupling of a weak relaxational mode to a polariton mode has never been discussed to our knowledge, we show that the effect can be explained through previously developed theories of polariton dispersion.[13,21] We begin with a standard treatment of a single-polariton mode, and then include coupling to a relaxational mode. This permits an analysis of the heterodyning of ISRS signals at large wave vectors and the higher than predicted damping rate in the time dependent signal at lower wave vectors. We finally include coupling between the polariton mode and other oscillatory modes to yield an understanding of peaks in the polariton damping rate at intermediate values of q.

A. Single polar mode

The following system of equations can be utilized to develop a dispersion relation for a single polar mode in a cubic crystal:[21]

$$(-\omega^2-i\omega\Gamma_1-B^{11})\mathbf{Q}_1=B^{1E}\mathbf{E}\ , \tag{15}$$

$$\mathbf{P}=B^{E1}\mathbf{Q}_1+B^{EE}\mathbf{E}\ , \tag{16}$$

$$\mathbf{E}=\frac{4\pi}{n^2-1}\mathbf{P}_T-4\pi\mathbf{P}_L\ . \tag{17}$$

Here $\mathbf{Q}_1$ is the vibrational coordinate, $\mathbf{E}$ is the electric field, n is the index of refraction, $\mathbf{P}$ is the polarization (with transverse component $\mathbf{P}_T$ and longitudinal component $\mathbf{P}_L$) and the B's are coupling constants. The polariton is modeled as a driven harmonic oscillator where ω_1 and Γ_1 are the natural frequency and decay rate of the pure transverse mode. The values of the coupling constants are found by solving for n^2 for a pure transverse mode ($P_L=0$) and comparing to the following phenomenological expression for the index of refraction:

$$n^2=\varepsilon_\infty+\frac{\omega_1^2(\varepsilon_0-\varepsilon_\infty)}{\omega_1^2-\omega^2-i\omega\Gamma_1}\ , \tag{18a}$$

where ε_0 and ε_∞ are the low and high limits of the frequency-dependent dielectric constant. We then find that

$$B^{11}=-\omega_1^2\ , \tag{18b}$$

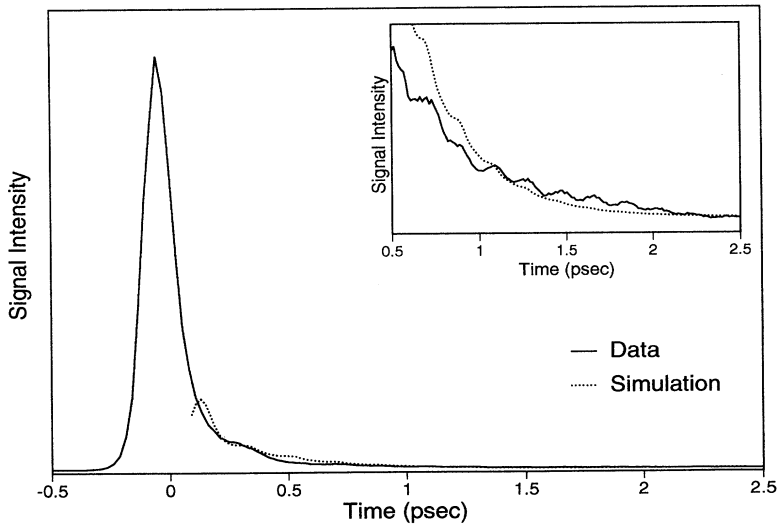

FIG. 4. ISRS signal from the A_1 polariton at $q=12\,800\ \mathrm{cm}^{-1}$. The signal can no longer be represented as a single oscillator, as evidenced by a nonexponential decay and clear heterodyning of the oscillatory signal. The signal oscillations now appear at the fundamental polariton frequency ω_p and not at $2\omega_p$ as at low wave vectors.

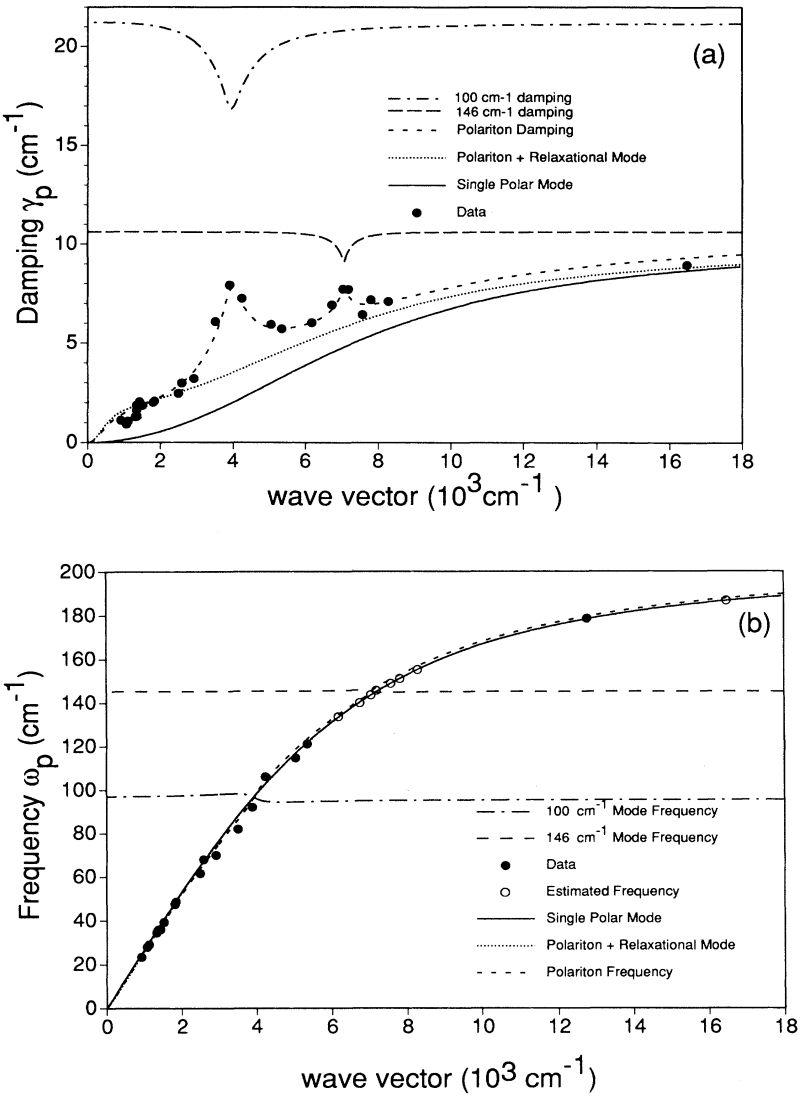

FIG. 5. (a) Wave-vector-dependent damping rate γ_p (half width at half maximum of the linewidth) of the polariton mode along with the dispersion curve predicted for the various models used. The legend is given in the figure. For a single polar mode (described in Sec. V A), strong deviations from the predicted results are observed, with the greatest deviations occurring below $q=2000$ cm^{-1}. The parameters used in the simulation are $\omega_1=201$ cm^{-1}, $\Gamma_1=20.2$ cm^{-1}, $\omega_L=402$ cm^{-1}, $\varepsilon'_\infty=8.5$. The polariton-relaxational mode damping dispersion curve predicted with inclusion of coupling to a weakly Raman-active relaxational mode (described in Sec. V B 1) shows much better agreement with the data in the low and high wave-vector ranges ($q<2000$ cm^{-1} and $q>9000$ cm^{-1}). The parameters used in the simulation are $\omega_1=201$ cm^{-1}, $\Gamma_1=14.9$ cm^{-1}, $\omega_L=402$ cm^{-1}, $\varepsilon'_\infty=8.5$, $\tau=0.3$ psec, $B^{1r}B^{r1}=1.1\times10^4$ cm^{-2}. The predicted damping dispersion for coupling to two additional oscillatory modes is denoted by polariton damping and shows excellent agreement with the data. The parameters used in the simulation are $\omega_1=201$ cm^{-1}, $\Gamma_1=16.4$ cm^{-1}, $\omega_L=402$ cm^{-1}, $\varepsilon'_\infty=8.5$, $\omega_2=99.7$ cm^{-1}, $\Gamma_2=42.4$ cm^{-1}, $B^{12}B^{21}=9.5\times10^{10}$ cm^{-4}, $\omega_3=145.9$ cm^{-1}, $\Gamma_3=21.2$ cm^{-1}, $B^{13}B^{31}=2.5\times10^{10}$ cm^{-4}, $\tau=0.3$ psec, $B^{1r}B^{r1}=9.6\times10^3$ cm^{-2}. (b) Wave-vector-dependent polariton frequency ω_p along with the frequency dispersion curves predicted for the models listed above. The predicted frequency dispersion curves remain essentially unchanged.

$$4\pi B^{1E}B^{E1}=\omega_1^2(\epsilon_0-\epsilon_\infty)\ , \tag{18c}$$

$$4\pi B^{EE}=\epsilon_\infty-1\ . \tag{18d}$$

(Reference 13 gives a complete treatment of the derivation.) Elimination of **E**, **P**, and **Q** and use of the relation $n=cq/\omega$ yields the dispersion equation

$$\omega^4+\omega^3(i\Gamma)-\omega^2\frac{c^2q^2+\omega_1^2\varepsilon_0}{\varepsilon_\infty}-\omega\frac{i\Gamma c^2q^2}{\varepsilon_\infty}+\frac{\omega_1^2c^2q^2}{\varepsilon_\infty}=0\ . \tag{19}$$

The relation between the high- and low-frequency dielectric constant values to the longitudinal and transverse phonon frequencies ω_L and ω_1 (usually labeled as ω_T), respectively, can be derived through Eqs. (15)–(18) and yields the familiar Lyddane-Sachs-Teller relation:

$$\varepsilon_0=\varepsilon_\infty\frac{\omega_L^2}{\omega_1^2}\ . \tag{20}$$

In $LiTaO_3$, ω_L for the first polar mode is equal to 402 cm^{-1} (Ref. 2). For the remainder of this work, we utilize the following modified value of ε_∞ (henceforth to be referred to as ε'_∞) to include the contribution to the dielectric constant from all higher-frequency optic modes along with the electronic contribution:[13]

$$\varepsilon'_\infty=\varepsilon_\infty\prod_{j=2}^{n}\frac{\omega_{Lj}^2}{\omega_{Tj}^2}\ . \tag{21}$$

For the low-frequency modes probed by experiments, $LiTaO_3$ can be approximated with a single polar mode model with ε'_∞ substituted for ε_∞ in Eq. (19).[13] Assuming an underdamped response for the A_1 phonon polariton at all wave vectors, which is evident from this and earlier work,[2,4–10] the roots of the polynomial can be found by assuming $\omega=-i\gamma_p\pm\omega_p$, where ω_p and γ_p are the frequency and damping rate of mode p. The four solutions to the dispersion relation can be separated into two pairs of roots, with each pair representing the fre-

quency and damping rate for the low- and high-frequency modes that satisfy the dispersion relation. However, only the low-frequency phonon in $LiTaO_3$ is within the bandwidth of our pulses. For the remainder of this paper, ω_p and γ_p represent the experimentally observed frequency and decay rate of the A_1 polariton at a given wave vector q. The roots of the dispersion relation representing the ω_p and γ_p values for the polariton are shown in Fig. 5 along with the experimental data.

It can be seen from Fig. 5(b) that the single-mode model yields a good description of the experimentally observed frequencies, but Fig. 5(a) shows a large disparity between the observed and predicted damping rates. There are two strong peaks in the damping rate at wave vectors corresponding to polariton frequencies of 92 and 146 cm^{-1}. However, the greatest deviation from the model occurs at the lowest wave vectors ($q < 2000$ cm^{-1}) where the experimentally observed damping rate is as much as seven times greater than predicted. No data points for the damping rate between $q = 10\,000$ and $q = 16\,000$ cm^{-1} are shown because the weak oscillatory signals in this region made accurate fitting of the data difficult. In the wave-vector range of $q = 6000$ cm^{-1} and $q = 9000$ cm^{-1}, where oscillations could not be time resolved, the data could still be fit well to single exponential decays. In the fitting procedure, we used the q-dependent values of the polariton frequency predicted by the theoretical dispersion curve. This is justified since the experimentally measured polariton frequencies both above and below this wave-vector range fall on the predicted dispersion curve. The damping rates determined through the fitting procedure were insensitive to substantial (i.e., at least 10%) variations in the assumed frequencies. All frequencies that were assumed are labeled as such on the dispersion figures.

For wave vectors below $q = 6000$ cm^{-1}, we estimate about $\pm 2\%$ uncertainties in the frequency and damping rate values. In the intermediate wave-vector region where the frequencies were taken from the dispersion curve, we estimate uncertainty in the damping rates to be $\pm 5\%$. In the high-q region where frequencies could again be measured directly, we estimate their uncertainties to be $\pm 5\%$.

B. Coupling to relaxational modes

1. *Effect of a coupled relaxational mode on damping rates*

Coupling of the polariton mode to a relaxational mode can explain both the high damping at low wave vectors ($q < 2000$ cm^{-1}) and the wave-vector-dependent heterodyning effects. A new dispersion relation can be derived through the use of Eqs. (16) and (17) and the following equations which represent the bilinear coupling of a relaxational mode to the polar optic mode:

$$(-\omega^2 - i\omega\Gamma_1 + \omega_1^2)\mathbf{Q}_1 = B^{1E}\mathbf{E} + B^{1r}\mathbf{Q}_r \,, \tag{22}$$

$$(1 - i\omega\tau)\mathbf{Q}_r = B^{r1}\mathbf{Q}_1 \,, \tag{23}$$

where τ is the decay time of the relaxational mode and B^{r1} and B^{1r} are the coupling constants. $\mathbf{Q}_r$ is assumed to have negligible contribution to the polarization relative to the polariton, which is reasonable due to the lack of scattering from the relaxational mode. Eliminating unknowns as before yields the following dispersion relation:

$$\omega^5 + iS\omega^4 - T\omega^3 - iX\omega^2 + Y\omega + iZ = 0 \,, \tag{24}$$

where

$$S = \tau^{-1} + \Gamma_1 \,,$$

$$T = \frac{c^2q^2}{\varepsilon_\infty} + \frac{\omega_1^2\varepsilon_0}{\varepsilon_\infty} + \frac{\Gamma_1}{\tau} \,,$$

$$X = \frac{c^2q^2}{\varepsilon_\infty\tau} + \frac{\Gamma_1 c^2q^2}{\varepsilon_\infty} - \frac{B^{1r}B^{r1}}{\tau} + \frac{\omega_1^2\varepsilon_0}{\varepsilon_\infty\tau} \,,$$

$$Y = \frac{\Gamma_1 c^2q^2}{\varepsilon_\infty\tau} + \frac{\omega_1^2 c^2q^2}{\varepsilon_\infty} \,,$$

$$Z = \frac{c^2q^2}{\varepsilon_\infty\tau}(\omega_1^2 - B^{1r}B^{r1}) \,.$$

The best fit to the experimentally observed frequency and damping dispersion of the polariton with Eq. (24) is shown in Figs. 5(a) and 5(b). The parameters that were used are given in the figure caption. Inclusion of the coupled relaxational mode introduces two new parameters, the relaxation time τ and the coupling constant product $B^{1r}B^{r1}$. The frequency dispersion curve is essentially unchanged, but the damping dispersion shows much better agreement with the experimental results in the low-frequency regime.

2. *Appearance of heterodyning at high wave vectors*

Coupling of the polariton to a relaxational mode not only explains the anomalously high polariton damping rate at low wave vectors but also explains the unusual observation of heterodyning at large wave vectors only. To quantify this, we calculate the q dependence in the relative contributions of the two modes to ISRS signal, including the effects of convolution over the pump and probe-pulse profiles.

In order to calculate the wave-vector dependence of the amplitude terms, we must derive the Green's function describing the material response from the dispersion relation given in Eq. (24). A similar derivation has been presented for a single polar mode with no relaxational contribution.[13] Equations (22), (23), together with Eqs. (16) and (17) can be rewritten as

$$\begin{bmatrix} -\omega^2 - i\omega\Gamma + \omega_1^2 & -B^{1r} & -\dfrac{4\pi B^{1E}}{n^2-1} \\ -B^{r1} & 1 - i\omega\tau & 0 \\ -B^{E1} & 0 & \dfrac{n^2-\varepsilon_\infty}{n^2-1} \end{bmatrix} \begin{bmatrix} \mathbf{Q}_1 \\ \mathbf{Q}_r \\ \mathbf{P} \end{bmatrix} = \begin{bmatrix} \mathbf{F}_1 \\ \mathbf{F}_2 \\ \mathbf{F}_3 \end{bmatrix} \,, \tag{25}$$

which has the form:

$$\mathbf{L}(\omega)\mathbf{X}(\omega)=\mathbf{F}(\omega)\ , \tag{26}$$

where $\mathbf{L}$ are linear operators, $\mathbf{X}$ are dynamic variables, and $\mathbf{F}$ are driving forces due to the ultrashort pulses. F_1 and F_2 represent the Raman scattering due to the oscillatory and relaxational mode, respectively, while F_3 represents the electro-optic effect. The Green's function is determined by

$$\mathbf{G}(\omega)=\mathbf{L}^{-1}(\omega)\ . \tag{27}$$

The inversion can be simplified if we can assume that $F_1 \gg F_2, F_3$. Similar experiments illustrate that the Raman effect dominates the electro-optic effect as an excitation mechanism,[13] justifying $F_1 \gg F_3$. From the form of the data, i.e., no direct observation of a relaxational mode is ever made, we can assume that $F_1 \gg F_2$. Also, as will be seen, the assumption is further supported by the agreement of the proposed model with experimental results. This means that $\mathbf{Q}(t)$ is dominated by $G_{11}(t)$ and $\mathbf{P}(t)$ is dominated by $G_{31}(t)$. As has been shown,[13] $G_{11}(\omega)$ and $G_{31}(\omega)$ are too similar to be distinguished in our experiments and we can assume that the ISRS signal is proportional to $|G_{11}(\omega)|^2$. Inverting $L(\omega)$ gives

$$G_{11}(\omega)=\frac{(c^2q^2-\varepsilon_\infty\omega^2)(1-i\omega\tau)}{Z}\ , \tag{28}$$

where Z is defined in Eq. (24). The Fourier transform of this relation yields

$$G_{11}(t)=\frac{1}{\tau\varepsilon_\infty}[K'e^{-\gamma_p t}\sin(\omega_0 t-\delta)-L'e^{-\lambda t}]\ , \tag{29}$$

where

$$\delta=\tan^{-1}\left[\frac{AC+BD}{AD-BC}\right]\ ,$$

$$K'=\frac{2[(AC+BD)^2+(AD-BC)^2]^{1/2}}{C^2+D^2}\ ,$$

$$L'=\frac{(1-\lambda\tau)(c^2q^2-\lambda^2\varepsilon_\infty)}{E}\ ,$$

$$A=(1-\gamma_p\tau)[c^2q^2-\varepsilon_\infty(\omega_p^2-\gamma_p^2)]+2\omega_p^2\gamma_p\tau\varepsilon_\infty\ ,$$

$$B=2\omega_p\gamma_p\varepsilon_\infty(1-\gamma_p\tau)+\omega_p\tau[c^2q^2-\varepsilon_\infty(\omega_p^2-\gamma_p^2)]\ ,$$

$$C=2\omega_p^2[(\omega_p^2-\omega_h^2)-(\gamma_p-\gamma_h)^2]$$
$$-4\omega_p^2(\gamma_p-\gamma_h)(\gamma_h-\lambda)\ ,$$

$$D=-2\omega_p\{(\gamma_p-\lambda)[(\omega_p^2-\omega_h^2)-(\gamma_p-\gamma_h)^2]$$
$$+2\omega_p^2(\gamma_p-\gamma_h)\}\ ,$$

$$E=[\omega_p^2-(\gamma_p-\lambda)^2][\omega_h^2+(\gamma_h-\lambda)^2]\ .$$

Here, λ is the wave-vector-dependent decay rate of the relaxational mode (τ is the uncoupled decay time, as discussed above), ω_p and γ_p are the coupled frequency and damping of the polariton, and ω_h and γ_h are the wave-vector-dependent values for the high-frequency solution to the dispersion relation which is not observed experimentally because it is outside the bandwidth of our pulses. Notice the dependence of the amplitude terms, K' and L', on the wave vector q. K' and L' depend both implicitly and explicitly on the wave vector q. Convolution over the excitation pulse duration is necessary for accurate determination of the relative amplitudes of the relaxational mode and the oscillatory term. As may be seen in Eq. (12), the convoluted amplitudes for $t \gg \tau_{\text{pulse}}$ are

$$K''=K'\exp\left[\frac{\tau_{\text{pulse}}^2(\gamma_p^2-\omega_p^2)}{4}\right]$$
$$\approx K'\exp\left[\frac{-\tau_{\text{pulse}}^2\omega_p^2}{4}\right]\ ,$$

$$L''=L'\exp\left[\frac{\lambda^2\tau_{\text{pulse}}^2}{4}\right]\ , \tag{30}$$

where the α's in Eq. (12) have been replaced with p's to represent the polariton frequency and damping, and the approximate expressions are based on the same assumptions described after Eq. (12). The convolution has little effect on the relaxational amplitude, since the relaxation time is long compared to the pulse duration (i.e., $\lambda\tau_{\text{pulse}} \ll 1$). However, since the frequency of the oscillatory term increases dramatically with wave vector, the convolution effects play a large role in the amplitude of the polariton term. The results are plotted in Fig. 6(a). The amplitudes of both terms decrease rapidly for wave-vector values below 1000 cm^{-1}, which is consistent with the decrease in signal at small wave vectors. This may be explained by the fact that at low wave vectors the low-frequency phonon-polariton brach becomes more light-like, while the higher-frequency branch becomes more phononlike and therefore more strongly Raman active. ISRS excitation and probing would couple more strongly to the higher-frequency branch, but since the frequency exceeds that of the 402 cm^{-1} longitudinal mode, it is outside of our accessible frequency range. At $q > 1000$ cm^{-1}, the relaxational amplitude exhibits little dispersion, but the oscillatory signal continues to increase until approximately $q = 5000$ cm^{-1}. The increasing frequency of the polariton then results in a gradual decrease in its amplitude. Note that even though the amplitudes of both terms decrease at low wave vectors, the relaxational mode amplitude is always at least a factor of 9 less than the oscillatory mode amplitude.

The parameters K' and L' and K'' and L'' measure the extent to which the vibrational and relaxational responses are induced by the excitation pulses, with the finite excitation pulse duration accounted for in K'' and L''. However, as discussed earlier and indicated in Eq. (10), ISRS signal depends on the square of the total response (including the excitation pulse convolution), convoluted with the probe-pulse temporal profile. The result, shown in Eq. (13), contains three terms which may be labeled K^2, KL, and L^2 and which include multiplicative factors which modify their relative intensities depending on the pulse durations and the values of the dynamical parameters (frequency and decay rates). The multiplicative factor for the term oscillating at $2\omega_p$ (the K^2 term) is

$$\exp\left[\frac{3(\gamma_p^2-\omega_p^2)\tau_{\text{pulse}}^2}{2}\right]\approx\exp\left[\frac{-3\omega_p^2\tau_{\text{pulse}}^2}{2}\right] \quad (31)$$

and for the term oscillating at ω_p (the KL term) is

$$\exp\left[\frac{\lambda\gamma_p\tau_{\text{pulse}}^2}{2}+\frac{\lambda^2\tau_{\text{pulse}}^2}{4}+\frac{(\gamma_p^2-\omega_p^2)\tau_{\text{pulse}}^2}{2}\right]\approx\exp\left[-\frac{\omega_p^2\tau_{\text{pulse}}^2}{2}\right]. \quad (32)$$

The relative ISRS signal intensities of the two terms are plotted in Fig. 6(b). Although the extent to which the two responses are driven by the excitation pulses, represented by K'' and L'' and shown in Fig. 7(a) varies little with q above 5000 cm^{-1}, we see that due to the finite probe-pulse duration the relative contributions to the two terms varies considerably. At low wave vectors, the K^2 term which oscillates at $2\omega_p$ overwhelms that of the relaxational mode. However, as the frequency of the mode grows with increasing wave vector, the time resolution of the experiment is no longer sufficient to detect the oscillations at $2\omega_p$. The ability of the probe to resolve the $2\omega_p$ term is diminished at about $q=6000$ cm^{-1}, in excellent agreement with the data. It is important to emphasize that this does not mean that there is no contribution to the data from the $2\omega_p$ term, but only that the response will appear as a single exponential decay due to differences in what can be driven by the excitation pulses and what can be time resolved by the probe pulse. Only the term that oscillates at ω_p can be time resolved above approximately $q=6000$ cm^{-1}, but this term does not ap-

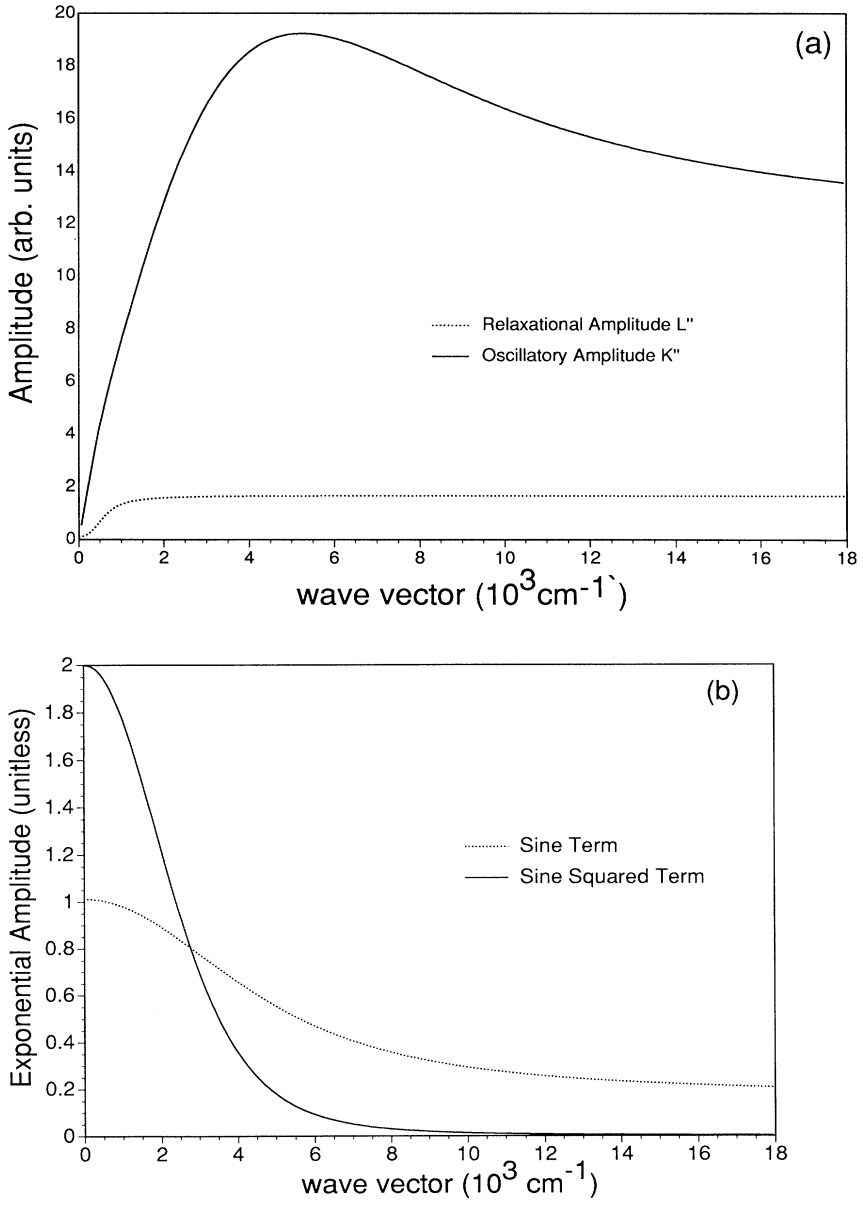

FIG. 6. (a) Wave-vector-dependent amplitude values for K'' and L'', including convolution over the excitation pulse duration. These plots show the extent to which the vibrational and relaxational modes are driven by the excitation pulses. The relaxational mode amplitude displays little dispersion, but the oscillatory mode amplitude shows a strong dependence on wave vector. (b) The effects of the probe pulse duration on the contributions of oscillatory and relaxational terms to ISRS data are shown. The convolution factors plotted are described in the text. The q-dependent ability of the probe to resolve signal oscillations at $2\omega_p$ compares very well to the experimental results. No oscillations at $2\omega_p$ are observed above $q=6000$ cm^{-1}.

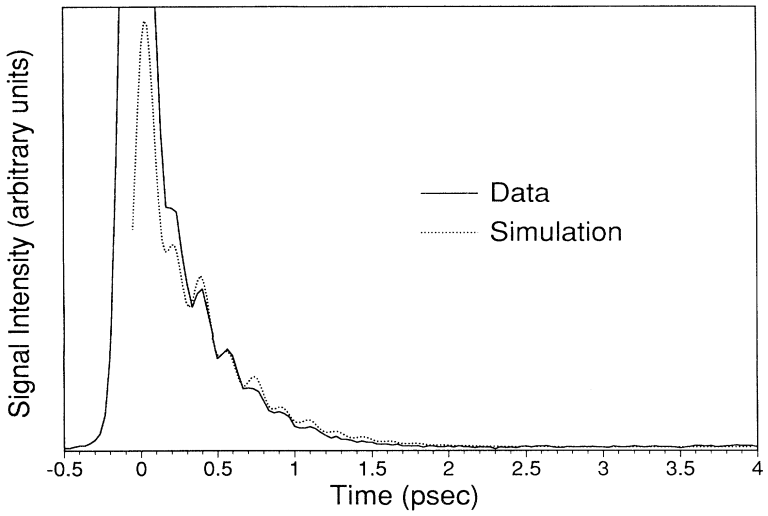

FIG. 7. The ISRS data at $q=3900\ \mathrm{cm}^{-1}$ where a peak in the experimentally observed damping is observed. The damped-oscillator simulation (with no adjustable parameters) illustrates that the signal can still be predicted based on the model and the data recorded at other wave vectors.

pear in the signal until higher wave vectors when the relative amplitude of the relaxational term is greater.

We can now obtain the expected time-dependent response for $q<2000\ \mathrm{cm}^{-1}$ and $q>9000\ \mathrm{cm}^{-1}$ by using the wave-vector-dependent Green's function given in Eq. (29) and the parameters used to generate the predicted dispersion curve in Fig. 5. The predicted time domain signals for two wave vectors discussed previously ($q=1800\ \mathrm{cm}^{-1}$ and $q=12\,800\ \mathrm{cm}^{-1}$) are shown in Figs. 2 and 4. Good agreement with the data is found. We emphasize that no new parameters are needed to accurately predict the time-dependent signal we observe. Only the parameters used to fit the dispersion curve are required. Little evidence for a heterodyne term is seen at low wave vectors where the signal oscillates at twice the frequency of the polariton and decays exponentially. The simulations show that at the higher wave vectors the signal oscillates at the frequency of the polariton with a nonexponential decay. The simulations are not meant to be fits to the data since all the parameters are not known with sufficient accuracy, but they reproduce the important features of the experimentally observed data in these regions.

An approximate value for the relaxation time τ of the coupled mode can be made from attempts at fitting the data at low wave vectors to the material response function stated in Eq. (9) for a damped harmonic oscillator and a relaxational mode. If a relaxation time longer than 0.3 ps is used, noticeable heterodyning of the signal at low wave vectors occurs in the simulation where the experimental results showed no heterodyne. If relaxation times shorter than this are used, the heterodyning observed in the data at the higher wave vectors does not occur. For the dispersion curves shown in Fig. 5 and all subsequent simulations, we used a value of 0.3 psec for the relaxation time of the mode. Note that τ, analogous to the phonon parameters ω_1 and Γ_1, describes the dynamics of the relaxational mode in the absence of coupling to the optic mode. However, the observed relaxation rate λ will display wave-vector-dependent decay rates at extremely small scattering angles (less than 0.25° assuming 615-nm excitation pulse).[13] The relaxation time observed in the wave-vector range of our experiments is therefore q independent.

Note that the treatment above is sufficient to rationalize the experimental results without introduction of any new parameters after the polariton dispersion is obtained from G_{11}, which is derived from Eq. (25). However, if the relaxational mode is due to "hopping" of ions (among different distinct potential energy minima in the unit cell), then it should be IR active. This gives rise to additional interactions with the phonon-polariton mode, i.e., in addition to the "mechanical" coupling to the ionic displacements represented by the coupling constants B^{1r} and B^{r1}, there is also coupling to the electric field which can be described by new coupling constants B^{rE} and B^{Er}. It is interesting to see whether our results, which we have rationalized in terms of exclusively mechanical coupling alternatively could be explained in terms of only coupling to the field. In this case Eq. (25) can be rewritten in the following way:

$$\begin{bmatrix} -(\omega_T^2-i\omega\Gamma_T-\omega^2) & 0 & \dfrac{4\pi B^{1E}}{n^2-1} \\ 0 & -(1-i\omega\tau_T) & \dfrac{4\pi B^{2E}}{n^2-1} \\ B^{E1} & B^{E2} & \dfrac{\varepsilon_\infty-n^2}{n^2-1} \end{bmatrix} \begin{bmatrix} Q_1 \\ Q_2 \\ P \end{bmatrix} = \begin{bmatrix} F_1 \\ F_2 \\ F_3 \end{bmatrix}, \tag{33}$$

where τ_T and τ_L represent the transverse and longitudinal relaxation times of the polar mode. The values $B^{1E}B^{E1}$ and $B^{2E}B^{E2}$ can be shown to be equal to

$$B^{1E}B^{E1}=\frac{\mathrm{Re}(C_1\omega_r^*)+i\omega\,\mathrm{Im}(C_1)}{4\pi}\ , \tag{34}$$

$$B^{2E}B^{E2}=\frac{\varepsilon_\infty\tau_T(\omega_L^2-\Gamma_L/\tau_T+1/\tau_T^2)(-1/\tau_T+1/\tau_L)}{4\pi(\omega_T^2-\Gamma_T/\tau_T+1/\tau_T^2)}\ , \tag{35}$$

where

$$C_1=\frac{\varepsilon_\infty(\omega_L^2-i\omega_r\Gamma_L-\omega_r^2)(\omega_r+i/\tau_L)}{(\omega_r+i/\tau_T)\mathrm{Re}(\omega_r)}$$

and

$$\omega_r=\frac{-i\Gamma_T}{2}+\sqrt{\omega_T^2-\Gamma_T^2/4}\ .$$

The dispersion curve of Fig. 5 can be reproduced almost identically for $\tau_T=0.30$ ps, $\tau_L=0.24$ ps, and $\Gamma_1=25.4$ cm^{-1}. *However, such a model does not simulate the time-dependent results well because the ratio of the amplitudes of the oscillatory to relaxational response is much too large.* Thus, the mechanical coupling model discussed up until this point models the time-dependent data well without any additional parameters, but the polar coupling model does require additional parameters. For example, the polar coupling model can reproduce the data if G_{22} is added to the response, which assumes a knowledge of the relative Raman cross sections of the oscillatory and relaxational responses. A value of 190 for this ratio can reproduce the time-dependent data reasonably well. Although the need for an additional parameter does not necessarily make this explanation incorrect, we feel that it is remarkable that the mechanical coupling model can reproduce the data equally well with no new parameters necessary after the generation of the dispersion curve.

C. Coupling to oscillatory modes

We now address the peaks in the damping rate which occur at polariton frequencies of 92 and 140 cm^{-1} ($q=3840$ cm^{-1} and $q=7000$ cm^{-1}). Figure 7 shows the data at $q=3900$ cm^{-1}, near the first peak. The signal is still that of a single exponentially decaying oscillatory mode as can be seen by the accompanying simulation. As shown in Table I, the peaks in the damping rate occur at polariton frequencies near the experimentally observed frequencies for previously assigned E-symmetry modes.[2,4–10] These E-symmetry modes have been shown to have some strain-induced A_1 symmetry character as discussed earlier. The following bilinear coupling model is used to simulate the response:

$$(-\omega^2-i\omega\Gamma_1+\omega_1^2)\mathbf{Q}_1=B^{1E}\mathbf{E}+B^{1r}\mathbf{Q}_r+B^{12}\mathbf{Q}_2+B^{13}\mathbf{Q}_3\ , \tag{36}$$

$$(-\omega^2-i\omega\Gamma_2+\omega_2^2)\mathbf{Q}_2=B^{21}\mathbf{Q}_1\ , \tag{37}$$

$$(-\omega^2-i\omega\Gamma_3+\omega_3^2)\mathbf{Q}_3=B^{31}\mathbf{Q}_1\ . \tag{38}$$

These expressions along with Eqs. (16), (17), and (23) may be used to derive a dispersion relation in a manner similar to that shown above. The relation is a ninth-order polynomial in ω. The full dispersion equation is not shown. The results of a fit to the experimental data points utilizing this dispersion relation are shown in Figs. 5(a) and 5(b) along with the parameters used. Three roots of the dispersion relation, which represent the damping rates and frequencies of the polariton and of the two E-symmetry modes, are shown. It should be pointed out that these curves represent the experimentally observable frequency and damping rates, and that the peaks in the damping dispersion curves are near avoided crossings of the different solutions of the ninth-order polynomial. The peaks in the damping dispersion curve occur when the frequency difference $\Delta\omega$ between the two modes whose crossing is avoided becomes smaller than the damping rate. The peaks are very strong indications of coupling of the phonon-polariton mode to other modes at the peak frequencies. Good agreement with the dispersion of the polariton damping rate is found, and the frequency dispersion curve remains essentially unchanged as observed experimentally.

The E-symmetry mode parameters that best reproduce the polariton damping dispersion curve are 100 and 146 cm^{-1} for the natural frequencies and 42 and 21 cm^{-1} for the full width at half maximum linewidths, respectively. Both values for the linewidths are roughly a factor of 2 greater than those found from previous experiments.[2,5,7] Because of the large linewidths it is difficult to eliminate two-phonon effects as a possible mechanism for the increased damping rates at these wave vectors. As stated previously, two-phonon effects have been proposed for a mode in the vicinity of 80 cm^{-1}, but never for the mode at 140 cm^{-1} (Ref. 10). As shown by the dispersion curves, we do not observe splittings in the frequency of the polariton at the damping peaks as is typical for strong Fermi resonances (i.e., two-phonon effects).[22,23] It is also possible that the mode at 92 cm^{-1} is different than the one previously assigned by others to be closer to 80 cm^{-1}. Auston and Nuss[11] recently observed a peak in the absorption of far-infrared light at a very similar frequency (90 cm^{-1}, in excellent agreement with our results) and proposed that a possible weak mode recently observed by others[24] was responsible. They suggested two-phonon effects due to the extreme weakness of the light-scattering intensity.

VI. MULTIPLE-PULSE ISRS EXPERIMENTS AT LOW TEMPERATURES

The relaxational mode to which the polariton is coupled most likely reflects thermally assisted "hopping" of the central Ta or Li ion among different local potential-energy minima within the unit cell. Analogous modes seen in simpler perovskite crystals including $KNbO_3$ and $BaTiO_3$ have been discussed extensively, and models have been proposed which describe the locations and energetics of the different minima.[19] As the temperature is re-

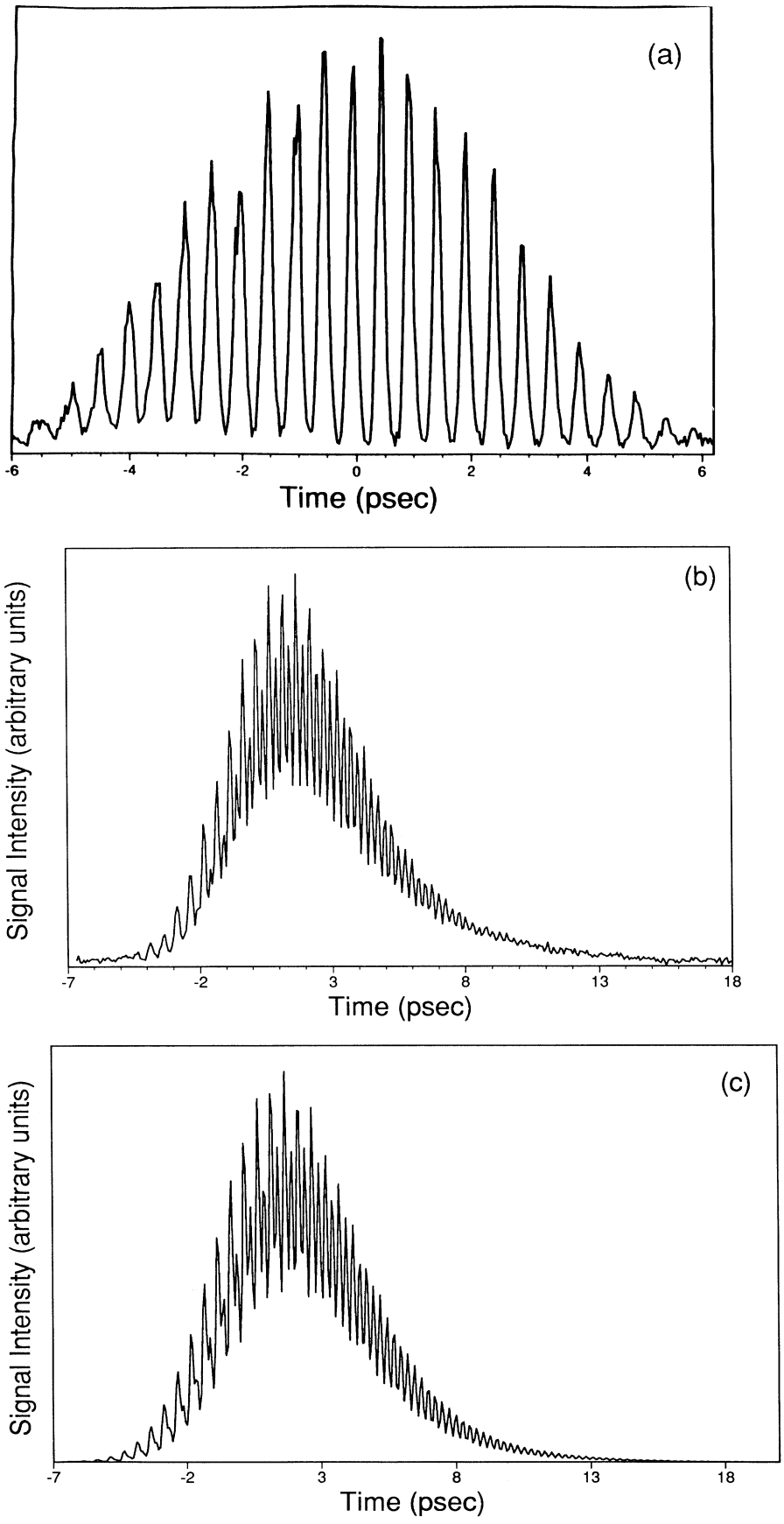

FIG. 8. (a) Cross correlation of a pulse train with 507 fs between successive pulses, used for multiple-pulse ISRS experiments. (b) Multiple-pulse ISRS data scan recorded at 120 K. (c) Simulation of the data scan assuming a Gaussian-shaped pulse train and a single harmonic oscillator response function.

duced, the hopping rate should decrease and the relaxational mode should be observed to decay more slowly. At the same time, the effects of coupling on the polariton mode should diminish due to the widening disparity between the dynamics of the two modes. Temperature-dependent ISRS studies were initiated to examine both the hopping dynamics and their influence on the polariton mode.

The experiments are made extremely difficult by the drastically reduced optical damage threshold of $LiTaO_3$ at low temperature. Photorefractive effects induced through two-photon absorption of the excitation pulses presumably occur at all temperatures, but at room temperature the effects are rapidly reversible.[25–27] At reduced temperatures they are very long-lived, and ISRS experiments with excitation pulses of sufficient intensity to generate detectable signals could not be conducted.

The use of a timed excitation pulse sequence instead of a single pair of excitation pulses has recently been demonstrated.[28,29] By timing a series of excitation pulses to match the polariton vibrational period, repetitive "impulse" driving forces are exerted which gradually build up an increased vibrational amplitude. In this manner the use of a single, intense pair of crossed excitation can be avoided. Since the damage is incurred through two-photon absorption rather than through linear absorption, the use of multiple-pulse excitation facilitates the low-temperature measurements. By reducing the peak excitation pulse intensity, the two-photon absorption probability was substantially reduced and multiple-pulse ISRS experiments could be carried out without photorefractive damage of the sample.

A typical data scan recorded at 120 K is shown in Fig. 8(b), along with a crosscorrelation of the pulse train with a single pulse [Fig. 8(a)]. For this data, the frequency and damping rate (expressed as a linewidth) of the polariton at 120 K with $q=2320$ cm^{-1} are 66 and 1.22 cm^{-1}, respectively. This compares to 64.5 and 2.48 cm^{-1} at room temperature. The reduced damping rate reflects the longer relaxational mode decay time and the consequently diminished influence of the relaxational mode on the polariton mode. We note that at this small wave vector, coupling only to the relaxational mode and not to the E-symmetry modes is of importance.

An approximate quantitative analysis of the polariton frequencies and damping rates determined at several reduced temperatures and several wave vectors can be attempted. We assume that the coupling constant between the polariton and relaxational mode (the B^{1r} term) does not change with temperature. This is reasonable since there are no structural phase transitions or other substantial temperature-dependent changes in the physical characteristics of the crystal. We use Raman linewidths determined previously[4] at a large scattering angle (therefore providing the phonon damping rates in the absence of polariton coupling) to generate theoretical phonon-polariton dispersion curves according to the single-mode model of Sec. V A. We then examine the measured temperature-dependent damping rates at various wave vectors. Any excess damping is ascribed to coupling to the relaxational mode, as in the room-temperature case. The procedure is illustrated below for 120 K.

At room temperature, a value of 15 cm^{-1} for the damping rate of the uncoupled phonon and coupling to a relaxational mode with a 0.3-ps decay time (with $B^{r1}B^{1r}=1.1\times10^4$ cm^{-2}) resulted in a total coupled phonon damping rate of approximately 20 cm^{-1} (at values of q that are large compared to the dispersion regime). From previous work,[4] a linewidth of 12 cm^{-1} (and a frequency $\omega_p=218$ cm^{-1}) at 80 K and 22 cm^{-1} at room temperature was found. We can extrapolate from these two values to estimate the damping rate and frequency of the uncoupled phonon at the intermediate temperatures. Figure 9 illustrates the polariton dispersion curve at 120 K predicted by Eq. (24). The parameters utilized are given in the figure caption. The decay time for the relaxational mode necessary to simulate the data ($\tau=0.6$ psec) is longer than at room temperature, as expected.

Similar measurements were taken at several temperatures and a plot of the relaxation time τ as a function of

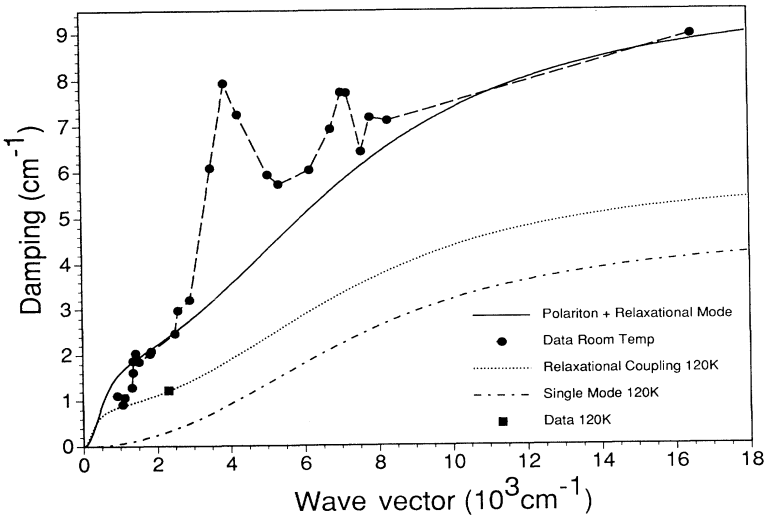

FIG. 9. Predicted and experimental dispersion of γ_p at room temperature and 120 K. The parameters used for the generated dispersion curve at 120 K with the relaxational mode included are $\omega_1=218$ cm^{-1}, $\Gamma_1=11$ cm^{-1}, $\varepsilon'_\infty=8.5$, $\omega_L=402$ cm^{-1}, $\tau=0.6$ psec, and $B^{1r}B^{r1}=1.1\times10^4$ cm^{-2}.

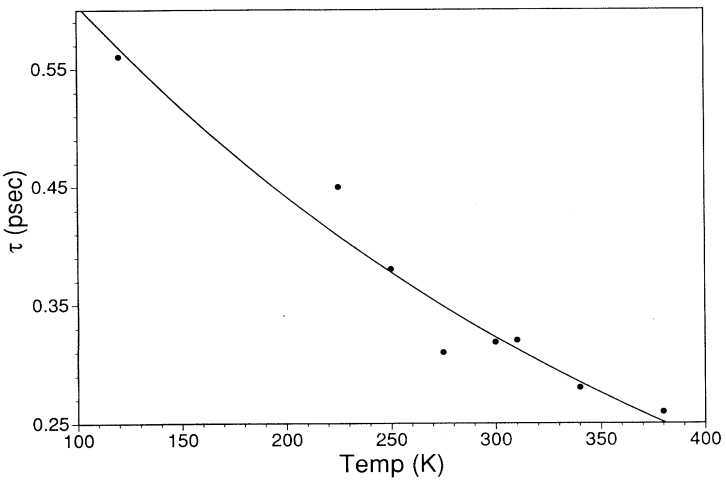

FIG. 10. A plot of the decay time τ of the weak relaxational mode in $LiTaO_3$. A monotonic increase in the decay time of the mode is observed as a function of temperature. The solid curve is an Arrhenius fit to the data with $\tau_0=0.9$ psec and $\Delta V=200\ \text{cm}^{-1}$.

temperature is given in Fig. 10. A monotonic increase in the relaxation time with decreasing temperature is observed. Considering the assumptions made above, we estimate that the values obtained for τ are accurate to within $\pm 30\%$. The main point is that the results are consistent with a thermally assisted hopping process coupled to the phonon-polariton mode. The relaxation times determined experimentally are shown along with a fit to an Arrhenius form

$$\tau=\tau_0 \exp\left[\frac{\Delta V}{kT}\right], \tag{39}$$

which yields the approximate parameters $\Delta V=200\ \text{cm}^{-1}$ and $\tau_0=0.9$ psec.

VII. CONCLUSIONS

A detailed ISRS study of the low-frequency lattice dynamics of $LiTaO_3$ has been carried out. The dispersion of the lowest-frequency A_1 phonon-polariton mode at room temperature has been determined. The wave-vector-dependent damping rates show strong deviations from those predicted for a single polar mode. At very low wave-vectors, the anomalously high polariton damping rate can be explained through coupling to a weakly Raman-active relaxational mode. The relaxational mode also accounts for unusual wave-vector-dependent heterodyning of the oscillatory ISRS signal. The dispersion of phonon-polariton and relaxational mode dynamical parameters and of the relative contributions of oscillatory and relaxational features to ISRS data were accounted for in quantitative calculation of the coupled-mode dispersion relation and simulation of the q-dependent ISRS data.

Strong peaks in the phonon-polariton damping rate near polariton frequencies of 92 and 140 cm^{-1} were also observed. These can be explained in terms of bilinear coupling to E-symmetry modes that possess some A_1 character due to strain in the crystal. No evidence was found for an avoided crossing which was previously reported to lead to splitting of the phonon-polariton frequency and time-dependent beating of the two resulting frequencies in the ISRS data.[14] We also do not see any evidence for a rising peak in the damping rate on either side of the reported avoided crossing, an easily discernible signature for this phenomenon in this experiment.

Multiple-pulse ISRS experiments were carried out at reduced temperatures, where ordinary ISRS experiments were frustrated due to photorefractive sample damage. Optical damage could be avoided through the use of multiple excitation pulses since the peak light intensity of any one pulse was greatly reduced. The results are consistent with coupling of the polariton mode to a relaxational ("hopping") mode whose decay rate decreases with temperature.

ACKNOWLEDGMENTS

This work was supported in part by ONR Grant No. N00014-92-1503. One of the authors (L.D.) was supported financially by the DoD and the AT&T Bell Laboratories Graduate Research Program for Women.

*Present address: Argonne National Laboratory, Chemistry Division, Bldg. 200, rm. E161, 9700 Cass Ave., Argonne, IL 60439.

†Present address: Department of Chemistry and Physics, Beaver College, Glenside, PA 19038.

‡Present address: Purdue University, School of Electrical Engineering, West Lafayette, IN 47907-1285.

[1] M. E. Lines and A. M. Glass, *Principles and Applications of Ferroelectrics and Related Materials* (Clarendon, Oxford, 1977).

[2] I. P. Kaminow and W. D. Johnston, Jr., Phys. Rev. **160**, 519 (1967).

[3] (a) T. P. Dougherty, G. P. Wiederrecht, and K. A. Nelson, Ferroelectrics **120**, 79 (1991). (b) T. P. Dougherty, G. P.

Wiedderecht, and K. A. Nelson, Science **258**, 770 (1992).
[4]W. D. Johnston, Jr. and I. P. Kaminow, Phys. Rev. **168**, 1045 (1968).
[5]A. S. Barker, Jr., A. A. Ballman, and J. A. Ditzenberger, Phys. Rev. B **2**, 4233 (1970).
[6]A. M. Glass and M. E. Lines, Phys. Rev. B **13**, 180 (1976).
[7]A. F. Penna, A. Chaves, P. da R. Andrade, and S. P. S. Porto, Phys. Rev. B **13**, 4907 (1976).
[8]A. Jayaraman and A. A. Ballman, J. Appl. Phys. **60**, 1208 (1986).
[9]X. Yang, G. Lan, B. Li, and H. Wang, Phys. Status Solidi B **141**, 287 (1987).
[10]C. Raptis, Phys. Rev. B **38**, 10 007 (1988).
[11]D. H. Auston and M. C. Nuss, IEEE J. Quant. Electron **24**, 184 (1988).
[12]M. C. Nuss and D. H. Auston, in *Ultrafast Phenomena V*, edited by G. R. Fleming and A. E. Siegman (Springer-Verlag, Berlin, 1986), p. 284.
[13]T. P. Dougherty, G. P. Wiederrecht, and K. A. Nelson, J. Opt. Soc. Am. B **9**, 2179 (1992).
[14]H. J. Bakker, S. Hunsche, and H. Kurz, Phys. Rev. Lett. **69**, 2823 (1992).
[15]Y.-X. Yan and K. A. Nelson, J. Chem. Phys. **87**, 6240 (1987).
[16]Y.-X. Yan and K. A. Nelson, J. Chem. Phys. **87**, 6257 (1987).
[17]Y.-X. Yan, E. B. Gamble, Jr., and K. A. Nelson, J. Chem. Phys. **83**, 5391 (1985).
[18]S. De. Silvestri *et al.*, Chem. Phys. Lett. **116**, 146 (1985).
[19](a) T. P. Dougherty, G. P. Wiederrecht, K. A. Nelson, M. H. Garrett, H. P. Jenssen, and C. Warde, Phys. Rev. B **50**, 8996 (1994). (b) P. C. M. Planken, L. D. Noordam, J. T. M. Kennis, and A. Lagendijk, Phys. Rev. B **45**, 7106 (1992). (c) P. Grenier, D. Houde, S. Jandl, and L. A. Boatner, *ibid.* **47**, 1 (1993).
[20]S. Ruhman, A. G. Joly, and K. A. Nelson, IEEE J. Quant. Electron. **24**, 460 (1988).
[21]R. Claus, L. Merten, and J. Brandmuuller, *Light Scattering by Phonon-Polaritons* (Springer-Verlag, Berlin, 1975).
[22]G. M. Gale, F. Vallee, and C. Flytzanis, Phys. Rev. Lett. **57**, 1867 (1986).
[23]F. Vallee, G. M. Gale, and C. Flytzanis, Phys. Rev. Lett. **61**, 2102 (1986).
[24]J. L. Servoin and F. Gervais, Solid State Commun. **31**, 387 (1979).
[25]E. Kratzig and R. Orlowski, Appl. Phys. **15**, 133 (1978).
[26]D. von er Linde, A. M. Glass, and K. F. Rodgers, J. Appl. Phys. **47**, 217 (1976).
[27]V. B. Batoev and E. M. Uyukin, Fiz. Tverd. Tela (Leningrad) **25**, 1222 (1983) [Sov. Phys. Solid State **25**, 702 (1983)].
[28]A. M. Weiner, D. E. Leaird, G. P. Wiederrecht, and K. A. Nelson, Science **247**, 1317 (1990).
[29]A. M. Weiner, D. E. Leaird, G. P. Wiederrecht, and K. A. Nelson, J. Opt. Soc. Am. B **5**, 1264 (1990).